Journal of Alloys and Compounds 509 (2011) 7324–7329

Contents lists available at ScienceDirect

Journal of Alloys and Compounds

journal homepage: www.elsevier.com/locate/jallcom

Diffusion bonding of Ti–2.5Al–2.5Mo–2.5Zr and Co–Cr–Mo alloys

Guo He*, Honghua Liu, Qingbiao Tan, Jiahua Ni

State Key Lab of Metal Matrix Composites, School of Materials Science and Engineering, Shanghai Jiao Tong University, 800 Dongchuan Road, Shanghai 200240, China

ARTICLE INFO

Article history:
Received 1 November 2010
Received in revised form 11 March 2011
Accepted 18 April 2011
Available online 23 April 2011

Keywords:
Biomaterials
Ti–2.5Al–2.5Mo–2.5Zr alloy
Co–Cr–Mo alloy
Dental alloy
Diffusion bonding

ABSTRACT

A solid state diffusion bonding between two metallic biomaterials, Ti–2.5Al–2.5Mo–2.5Zr alloy and Co–Cr–Mo alloy (F75), has been investigated by using energy-dispersive spectrometer analysis, metallographic observation and bonding strength evaluation. The experiments indicate that bonded at 750 °C leads to insufficient atoms diffusion and weak bond. When bonded at 900 °C some intermetallics, $CoTi_2$, Co_2Ti, and Cr_2Ti, form in the diffusion zone, which significantly deteriorate the plasticity and lead to lower bonding strength. A high bonding strength can be achieved when bonding at 850 °C for 60 min. During the bonding process each element exhibits various diffusion velocity in the opposite alloy. The diffusion coefficients for those elements can be ranked in following sequence: $D_{Co} > D_{Cr} > D_{Mo}$ in the Ti–2.5Al–2.5Mo–2.5Zr alloy and $D_{Ti} > D_{Al} > D_{Zr}$ in the Co–Cr–Mo alloy.

1. Introduction

Metallic biomaterials are frequently used as load bearing implants because they have higher mechanical properties. Among them cobalt–chromium alloys and titanium alloys are very popular in surgical practice [1]. Cobalt–chromium alloys have very good resistance to most forms of corrosion, including crevice corrosion and stress corrosion cracking. They also have good resistance to wear and excellent tribological properties [2]. These superiorities allow the cobalt–chromium alloys to be used for artificial joints or used in dentistry. Titanium alloys have good strength-to-weight ratios and excellent corrosion resistance to most environments likely to be found *in vivo* [3]. The elastic modulus of the titanium alloy is about half of those of stainless steels and cobalt–chromium alloys. Coupled with their excellent biocompatibility, titanium alloys have become attractive materials for medical devices. They are suitable for long-term implants such as the stem of artificial joints, the cover of cardiac pacemaker, and dental implants etc. [4,5].

Due to differences in mechanical properties and biocompatibilities, cobalt–chromium alloys and titanium alloys usually adapt to different situations when used as implants. For examples, cobalt–chromium alloys are felicitous for fabrication of crown due to their strong bonding with porcelain [6], whereas titanium alloys are most commonly used as dental implants including endosseous, subperiosteal, or transosteal in clinical practice [7]. When a totally dental restoration is needed, a bimetal tooth or denture perhaps is an optimum choice. Another example is that the artificial hip can be made of bimetals. The cobalt–chromium alloy with lower coefficient of friction is used as the ball and the socket of the hip joint [1], and the titanium alloy with lower elastic modulus is used as the hip stem [5]. Such bimetallic device has dual advantages: the cobalt–chromium alloy can slower wearing in the hip joint and the titanium alloy is easily coupled with the surrounding bone.

In order to construct a bimetallic device, one must apply a bonding process. Among various bonding technologies, solid state bonding is a better choice because there is no heat affected zone and small deformation. In this study, we demonstrate a solid state diffusion bonding between a cobalt–chromium–molybdenum alloy (meets ASTM standards Specification in F75) and a new titanium alloy which was developed in China for the surgical application.

2. Material and methods

A cast cobalt–chromium–molybdenum alloy rod with 10 mm in diameter was selected as raw material. Its chemical composition and physical properties are listed in Tables 1 and 2, respectively. The as-cast microstructure is composed of a solid solution matrix and grain boundary precipitates [8]. The matrix is a combination of two allotropic γ and ε phases. The γ is a face centered cubic (*fcc*) structure, which is stable above 970 °C, while the ε is a *hcp* structure, which is stable from room temperature to 970 °C. When heating the alloy, the metastable γ phase transforms into stable ε phase. The precipitates distributed in the matrix are discontinuous grain boundary carbides. Usually they are mixture of $M_{23}C_6$ carbides and *fcc* phase [9]. A Ti–2.5Al–2.5Mo–2.5Zr (in wt.%) alloy

* Corresponding author. Tel.: +86 21 3420 2643; fax: +86 21 3420 2643.
E-mail address: ghe@sjtu.edu.cn (G. He).

0925-8388/$ – see front matter © 2011 Elsevier B.V. All rights reserved.
doi:10.1016/j.jallcom.2011.04.098

Table 1
Chemical compositions of TAMZ and Co–Cr–Mo alloys (wt.%).

Alloys	Ti	Al	Mo	Zr	Co	Cr	Fe	Si	C	N	H	O
TAMZ	Bal.	2.5	2.5	2.5	–	–	0.3	0.15	0.1	0.05	0.1	0.15
Co–Cr–Mo	0.25	–	6	–	63.8	28.8	0.42	0.1	0.06	0.03	0.01	0.12

Table 2
Physical Properties of TAMZ and Co–Cr–Mo alloys.

Alloys	Melting point (°C)	Hardness (HV)	Elongation (%)
TAMZ	1450	268	13
Co–Cr–Mo	1380	380	6

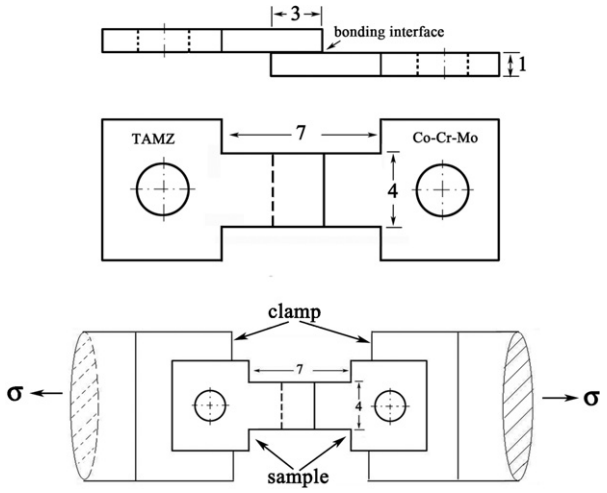

Fig. 1. Sample dimensions and the schematic illustration of the tensile shear test.

(TAMZ) sheet (its composition and physical properties are listed in Tables 1 and 2, respectively) was selected as a counterpart material. It was manufactured by hot rolling followed by vacuum annealing. Its microstructure is composed of equiaxed primary α grains and α + β eutectic phase [10].

Both alloys were machined into 'T-shape' pieces as illustrated in Fig. 1. Such shape is convenient to performing the tensile shear test after the bonding process. All the sample sizes are indicated in Fig. 1. Before bonding, the sample surface was burnished by using

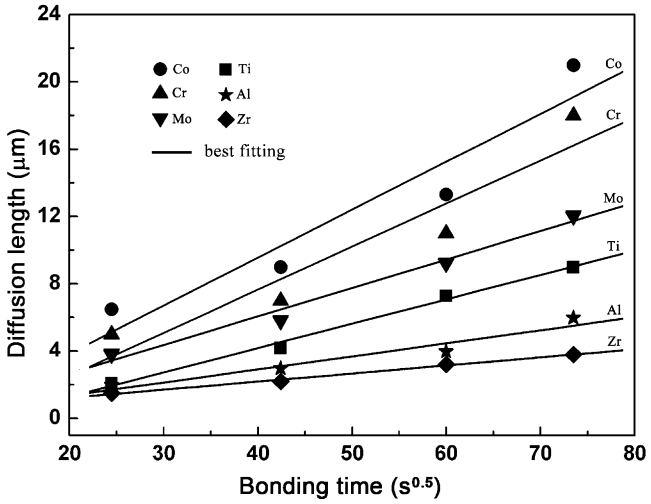

Fig. 2. Effect of bonding time on the diffusion length for bonding at 850 °C.

abrasive papers and polishing machine, then etched in a solution of 5 ml HNO_3 + 10 ml HF + 85 ml H_2O to remove face oxide and ultrasonically cleaned with ethanol for 5 min. The solid state bonding was processed in a vacuum chamber with 1×10^{-3} Pa pressure. The two 'T-shape' samples were mounted on a substrate in the chamber with 3 mm × 4 mm overlapping area as shown in Fig. 1. A constant stress of 3 MPa was applied on the bonding area to keep the two pieces in close contact. The bonding was performed by heating the sample set from room temperature up to a certain temperature and holding for the setting time, then cooling in the chamber to the room temperature. The heating rate is 25 °C/min. In order to investigate the effect of temperature and holding time on the diffusion bonding, four different temperatures: 750 °C, 800 °C, 850 °C, and 900 °C, and different holding time were demonstrated in this study.

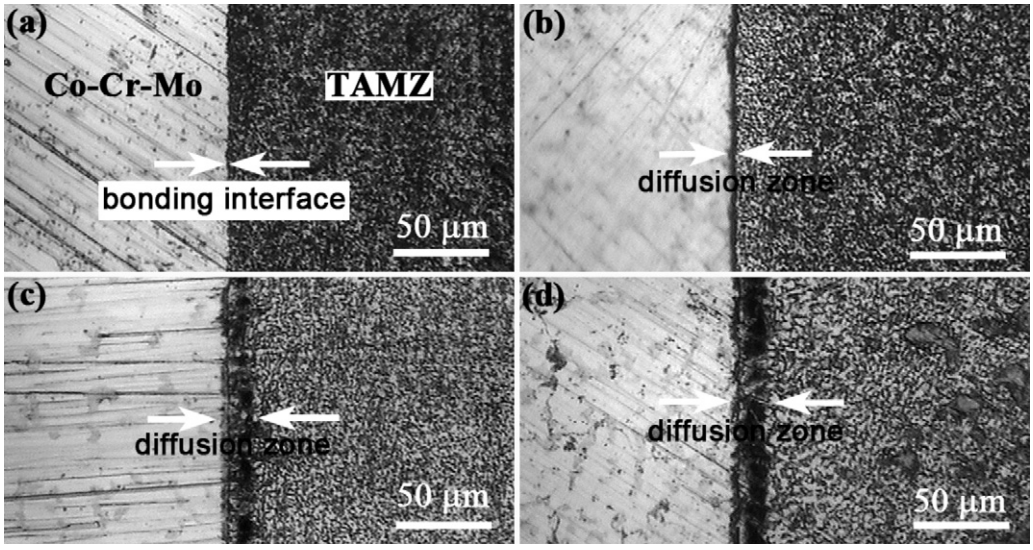

Fig. 3. Optical microstructures of the samples bonded at 850 °C for 10 min (a), 30 min (b), 60 min (c), and 90 min (d), respectively.

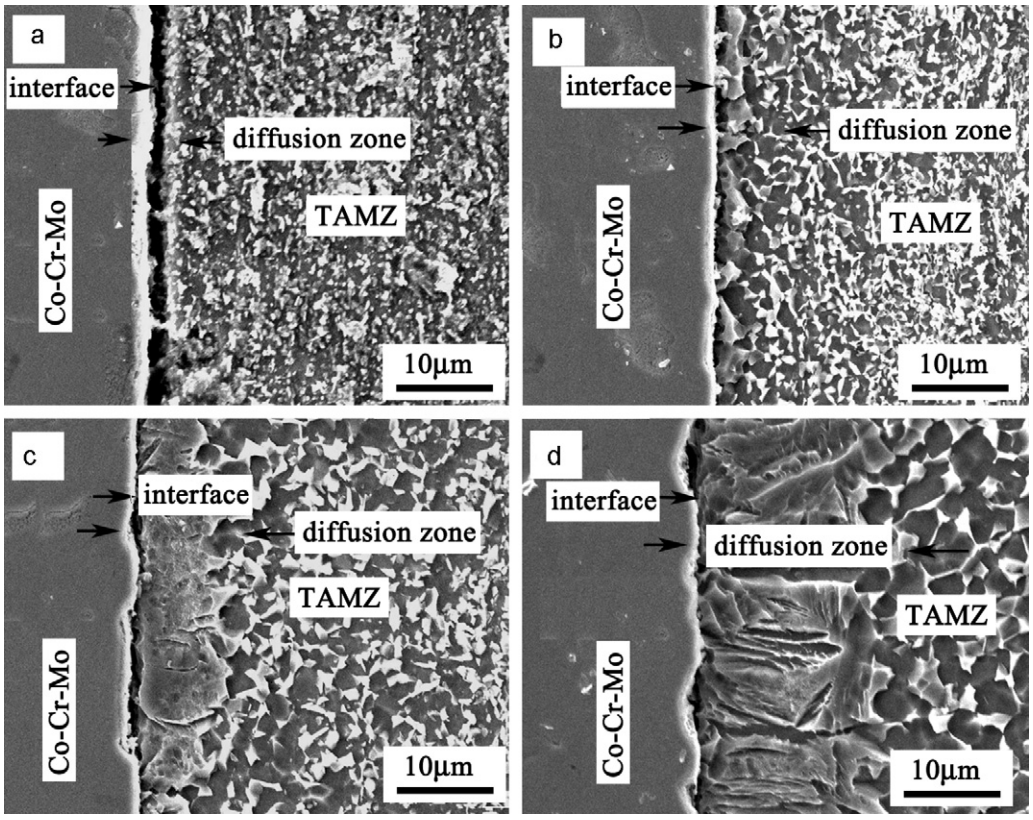

Fig. 4. SEM images of the samples bonded for 60 min at 750 °C (a), 800 °C (b), 850 °C (c), and 900 °C (d), respectively.

The bonded samples were metallographically characterized by using a Nikon EPIPHOT-300 microscope and a JEOL-JSM6460 scanning electron microscope (SEM) with an energy-dispersive spectrometer (EDS). The etching agent is Korll solution (6 ml HCl + 2 ml HF + 92 ml H_2O). In order to identify the phases in the diffusion zone, a Rigaku D/max-2550 X-ray diffraction (XRD) with Cu-Kα radiation (λ = 1.54184 Å) was used. The microhardness across the bonding interface was determined by using an Everone MH-6 micro sclerometer. The tensile shear strength of the bonded samples was evaluated by using AG-100KNA ShimaDzu testing

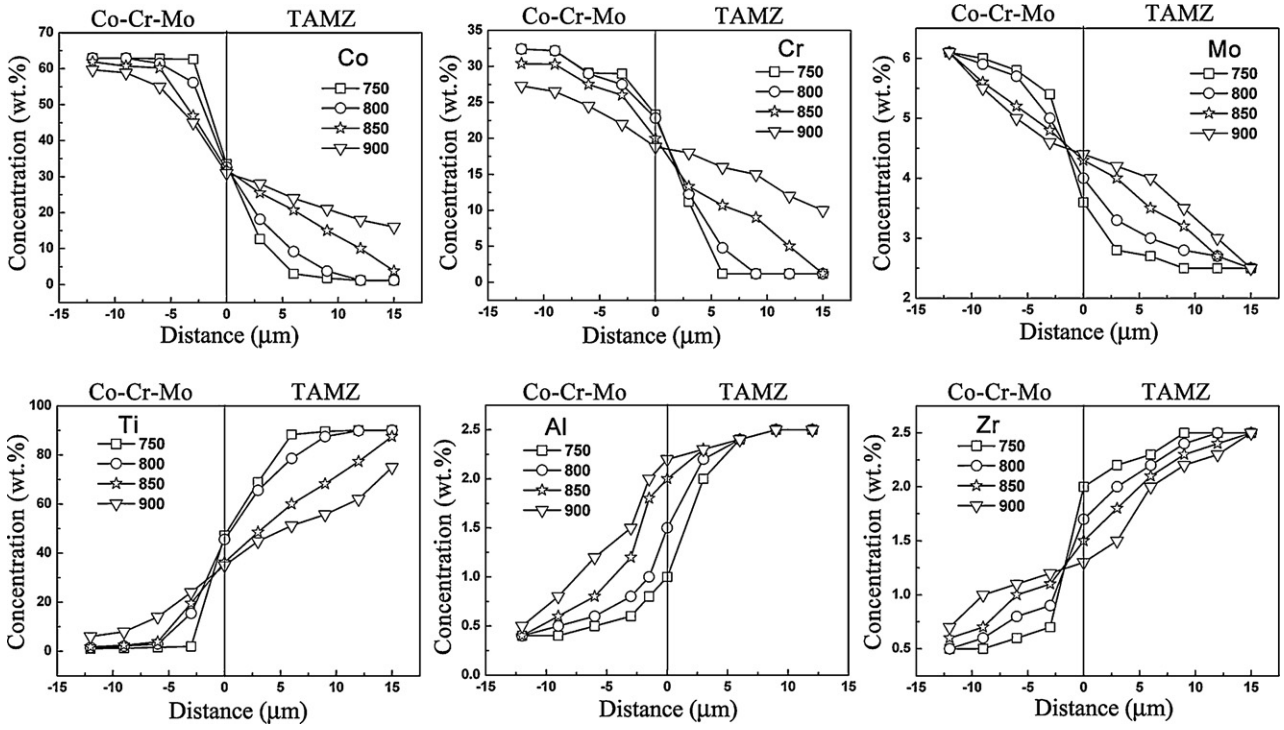

Fig. 5. Concentration profiles across the bonding interface.

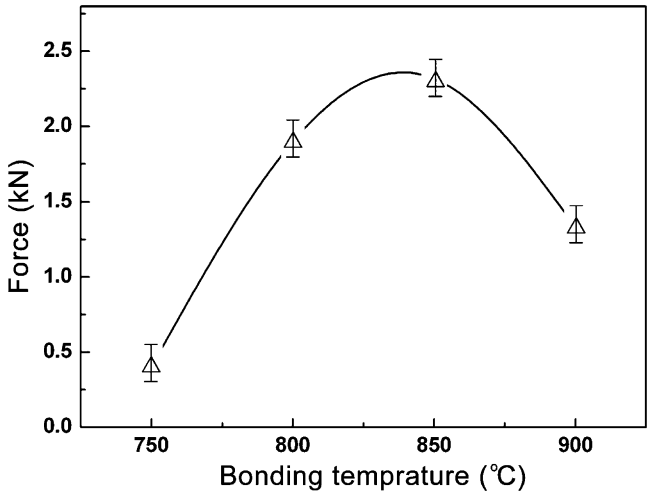

Fig. 6. Tensile shear force for the samples bonded at different temperature.

machine at room temperature. The cross-head speed for the tests is 0.01 mm/s. The reported tensile shear strength values in this paper are average values of at least three samples with the same diffusion bonding condition.

3. Results and discussion

3.1. Effect of bonding time on the atoms diffusion

A group of samples were bonded at 850 °C for 10 min, 30 min, 60 min, and 90 min, respectively. The metallographic observation and EDS analysis clearly reveal the solid state atoms diffusion between the two alloys. By means of EDS line scan analysis, the diffusion length of the main elements in the two alloys can be identified. Putting those data in the diffusion length-bonding time coordinates, a near lineal relationship between the diffusion length and the square root of the bonding time can be drawn as shown in Fig. 2. Those elements exhibit very different diffusion velocities in the opposite alloy. Co, Cr, and Mo diffuse in the Ti alloy much faster than Ti, Al, and Zr in the Co–Cr–Mo alloy. For a one-dimensional diffusion, the square of diffusion length, x, is directly proportional to the diffusion time, t, and the diffusion coefficient, D [11]:

$$x^2 \propto Dt \quad (1)$$

Therefore, a sequence of the diffusion coefficients for those elements can be drawn as: $D_{Co} > D_{Cr} > D_{Mo}$ in the TAMZ alloy and $D_{Ti} > D_{Al} > D_{Zr}$ in the Co–Cr–Mo alloy according to Fig. 2.

The atoms diffusion has induced some phase transformation (this phenomenon was confirmed by the XRD analysis, as stated in Section 3.3) in the TAMZ alloy. A fuscous layer near the bonding interface in the TAMZ side is visible as shown in Fig. 3b–d. With the increase in bonding time, the fuscous layer becomes wider. Longer bonding time allows more Co, Cr, and Mo into the TAMZ alloy and larger diffusion length in the TAMZ side, thus leads to phase transformation in a wider zone. Since Co, Cr, and Mo are β-formers in Ti alloy, the diffusion zone should comprise more fraction of β phase which is in dark-gray under the optic view as indicated by arrows in Fig. 3. In the side of the Co–Cr–Mo alloy, the microstructure does not show any changes, suggesting that the diffusion of Ti, Al, and Zr into the Co–Cr–Mo alloy does not induce obvious phase transformation. In addition, the bonding processing has lead to grain coarsening in the TAMZ parent alloy due to the recrystallization and grain growth in the high temperature. Longer bonding time leads to coarser microstructure as shown in Fig. 3.

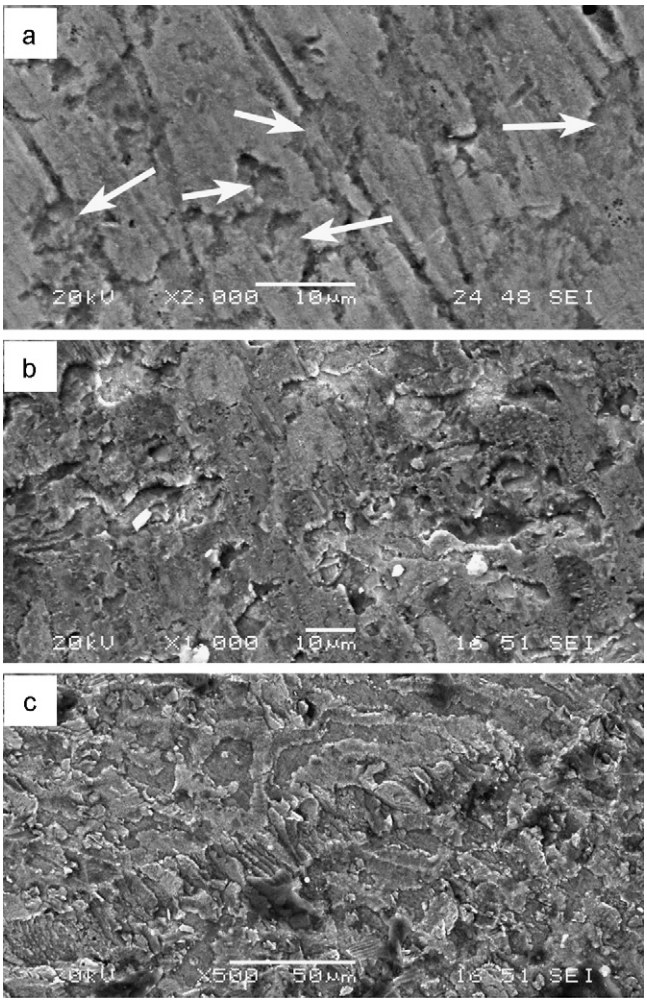

Fig. 7. Fractographs of the samples bonded for 60 min at 750 °C (a), 850 °C (b), and 900 °C (c), respectively.

3.2. Effect of temperature on the diffusion bonding

In order to investigate the effect of bonding temperature, the bonding processes were carried out at 750 °C, 800 °C, 850 °C, and 900 °C, respectively, for the same time 60 min. The bonded interfaces are shown in Fig. 4. A badly bonded interface with distinct vacancies appears in the samples bonded at 750 °C (Fig. 4a). It suggests that 750 °C is not enough to form an effective bond. Bonded at higher temperature, e.g., 800–900 °C, results in a closer bond (Fig. 4b–d). The atoms diffusion has induced significant changes in microstructure in the TAMZ side near the interface. This indirectly reveals the atoms diffusion length. Higher temperature corresponds to a larger diffusion length. In the diffusion zone, Co, Cr, and Mo with high concentrations improve to form β phase in the TAMZ alloy. This β phase displays a different morphology from that of the parent alloy (see Fig. 4c and d). The microstructure in the Co–Cr–Mo alloy near the interface does not show any change in these conditions even though some Ti, Al, and Zr atoms have diffused into the alloy. Additionally, bonding processing at high temperature has induced significant grain coarsening in TAMZ parent alloy as shown in Fig. 4. The higher bonding temperature corresponds to the coarser microstructure, because the higher temperature improves the recrystallization and the grain growth.

By means of EDS analysis, the concentration profiles for each element after the bonding process at different temperature were drawn in Fig. 5. The atoms diffusion length can be clearly shown in

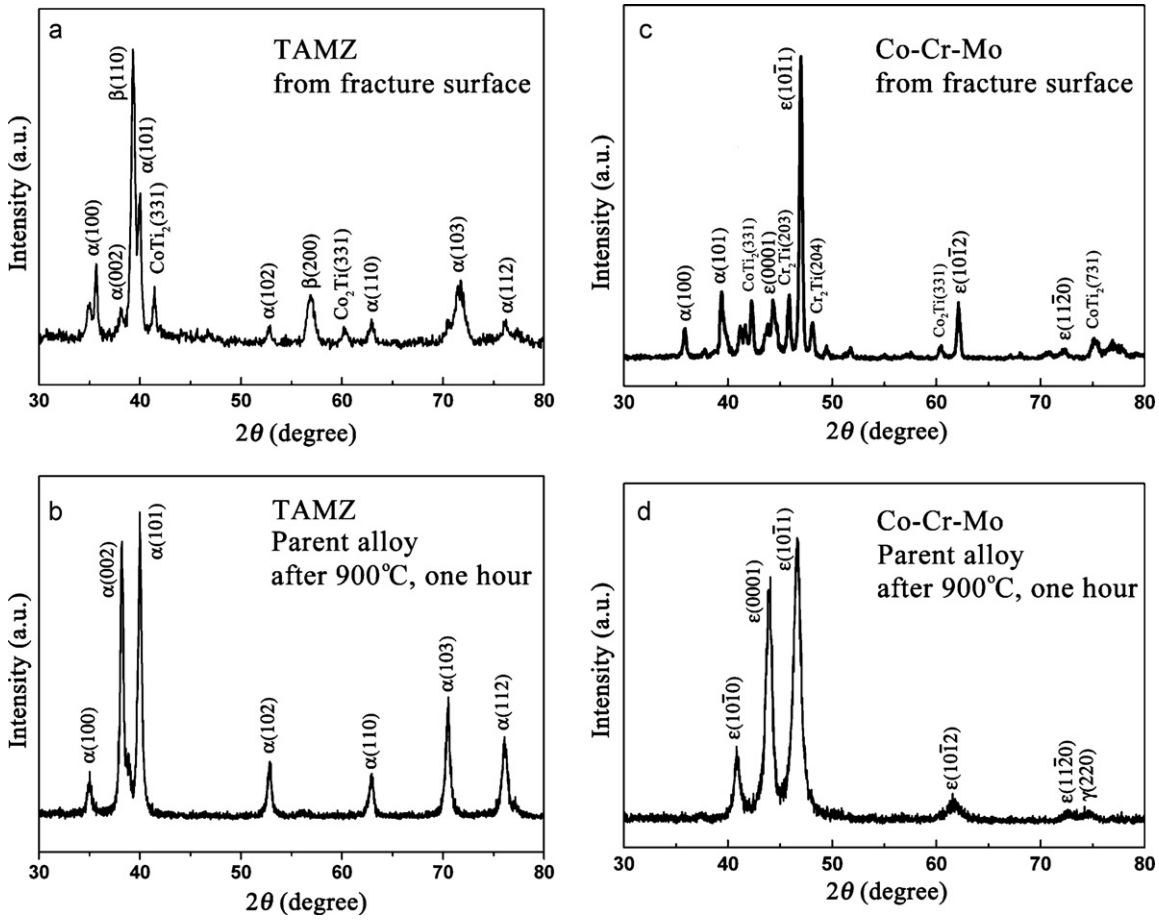

Fig. 8. X-ray diffraction patterns taken from the fracture surfaces (a and c) after bonding at 900 °C for 60 min, and from the parent alloys (b and d) after the bonding.

the graphs. The diffusion length of Co, Cr and Mo in the TAMZ alloy is about 5–8 μm when bonding at 750 °C for 60 min, but reaches about 15 μm when bonding at 850 °C for the same bonding time. When bonding at 900 °C the diffusion length of the Co and Cr far exceeds 15 μm. In the diffusion layer from zero to 15 μm the Co concentration reaches about 20–30%, and the Cr reaches about 10–18%. Referring to Ti–Co and Ti–Cr binary phase diagrams [12] such high concentrations of the Co and Cr can improve β transformation and induce forming Ti_2Co and Cr_2Ti intermetallics in the diffusion zone. In the side of the Co–Cr–Mo alloy, the diffusion length of Ti is very small when bonding at 750 °C for 60 min. The longest Ti diffusion length reaches about 10 μm and the highest Ti concentration near the bonding interface reaches about 20% when bonding at 900 °C for 60 min. The high Ti concentration may induce forming intermetallics in the Co–Cr–Mo alloy near the bonding interface. Although Al and Zr also diffuse into the Co–Cr–Mo alloy, the highest concentration is below 2.0% for Al and below 1.2 for Zr. Both the Al and Zr may act as alloying elements in the Co–Cr–Mo alloy to strengthen the material.

3.3. Bonding strength

The tensile shear tests indicate that the bonding at 750 °C for 60 min forms a very weak bond. Above 800 °C an effective bond can be achieved. A higher strength is obtained at 850 °C. Bonded at 900 °C the bonding becomes worse for the formation of intermetallics. Plotting the tensile shear force to the bonding temperature, a parabolic relationship can be clearly shown in Fig. 6. The maximum of the bonding strength appears at about 840 °C, suggesting that the best bonding temperature should be set as 840 °C when bonding time is 60 min.

The fracture surface after the tensile shear test has been carefully examined for understanding of the failure mechanism. The fractograph of the samples bonded at 750 °C shows some separated small area with 'peeling off' traces as indicated by white arrows in Fig. 7a. Most of the contact interface is not connected, resulting in a very weak bonding strength. For the samples bonded at 850 °C and 900 °C, the contact interface is completely bonded (Fig. 7b and c). The former exhibits a 'peeling off' mechanism in dominance (Fig. 7b) and the latter displays a 'tearing up' mechanism (Fig. 7c) which can be frequently found in the fractographs of Ti alloys with mixture of α or β and intermetallics [13–15]. Such mixed microstructure usually exhibits very limited plasticity.

The appearance of the intermetallics on the bonding interface can be detected by XRD analysis. The XRD patterns were taken from the fracture surface as shown in Fig. 8a (TAMZ side) and Fig. 8c (Co–Cr–Mo side). For comparison, the patterns taken from the parent alloys which have been heat treated at 900 °C for 60 min are also presented in Fig. 8b (for TAMZ) and Fig. 8d (for Co–Cr–Mo). Although only α phase can be detected in the TAMZ parent alloy, the strong peaks for β phase suggest α → β phase transformation in the diffusion zone close to the fracture surface as shown in Fig. 8a. Besides, $CoTi_2$ and Co_2Ti intermetallics and α phase also can be indexed in the patterns (Fig. 8a). In the side of the Co–Cr–Mo alloy, the stable ε phase dominates in the parent alloy (Fig. 8d), but several intermetallics, $CoTi_2$, Co_2Ti, and Cr_2Ti, can be indexed on the bonding interface close to the fracture surface (Fig. 8c). These intermetallics mixed with the α/β phase (for TAMZ alloy) and the ε

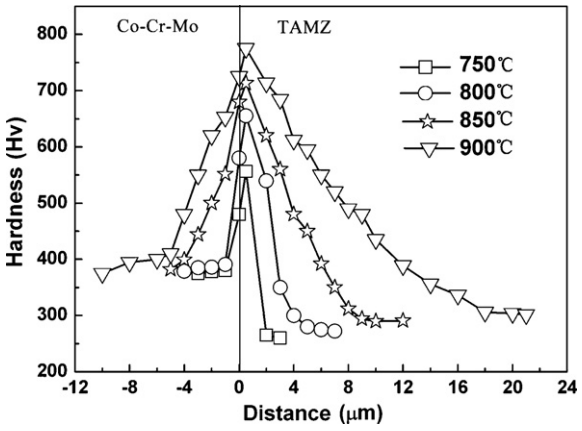

Fig. 9. Microhardness distribution across the interface bonded for 60 min at 750 °C (a), 800 °C (b), 850 °C (c), and 900 °C (d), respectively.

phase (for Co–Cr–Mo alloy) are expected to deteriorate plasticity and induce very high hardness.

The microhardness tests reveal that there is a gradient hardness distribution from the bonding interface towards the parent alloys as shown in Fig. 9. The high hardness appears on the bonding interface, which reaches about HV550 for the samples bonded at 750 °C and about HV760 for that bonded at 900 °C. The higher bonding temperature corresponds to the higher hardness and the wider distance where a gradient hardness distributes. Those values of the distances just match with the atoms diffusion lengths which have been evaluated by the EDS analysis (Fig. 5) and the metallographic observation (Fig. 4). The appearance of the intermetallics and the alloying effect in the diffusion zone contributes to the higher hardness.

4. Conclusion

(1) Ti–2.5Al–2.5Mo–2.5Zr alloy and Co–Cr–Mo alloy (F75) can be bonded successfully by solid state diffusion method. During the bonding process each element exhibits various diffusion velocity in the opposite alloy. The diffusion coefficients for those elements can be ranked in following sequence: $D_{Co} > D_{Cr} > D_{Mo}$ in the Ti–2.5Al–2.5Mo–2.5Zr alloy and $D_{Ti} > D_{Al} > D_{Zr}$ in the Co–Cr–Mo alloy.

(2) The solid state atoms diffusion strongly depends on the temperature and the holding time. When bonded at 850 °C, the proper bonding time is about 60 min. The higher bonding temperature can speed the atoms diffusion and shorten the bonding time, but may induce intermetallics formation near the interface, microstructure coarsening in the parent alloy and the possible oxidation for Ti alloys.

(3) A high bonding strength can be achieved when bonding at 850 °C for 60 min. Bonding at lower temperature leads to insufficient atoms diffusion and weak bond. Bonding at higher temperature results in the formation of $CoTi_2$, Co_2Ti, and Cr_2Ti in the diffusion zone, which significantly deteriorate the plasticity and lead to lower bonding strength.

Acknowledgement

The Ti–2.5Al–2.5Mo–2.5Zr alloy used in this study was provided by Northwest Institute for Non-ferrous Metal Research (NIN), China.

References

[1] S.H. Teoh, Engineering Materials for Biomedical Applications, World Scientific Publishing, Singapore, 2004.
[2] N.J. Hallab, R.M. Urban, J.J. Jacobs, Corrosion and biocompatibility of orthopedic implants, in: M.I. Yaszemski, D.J. Trantolo, V. Kai-Uwe Lewandrowski, D.E. Hasirci, D.L. Altobelli, Wise (Eds.), Biomaterials in Orthopedics, Marcel Dekker, New York, 2004, pp. 63–91.
[3] M. Niinomi, Mechanical properties of biomedical titanium alloys, Mater. Sci. Eng. A243 (2000) 231–236.
[4] M. Niinomi, T. Hattori, S. Niwa, Material characteristics and biocompatibility of low rigidity titanium alloys for biomedical applications, in: M.I. Yaszemski, D.J. Trantolo, Kai-Uwe Lewandrowski, V. Hasirci, D.E. Altobelli, D.L. Wise (Eds.), Biomaterials in Orthopedics, Marcel Dekker, New York, 2004, pp. 41–62.
[5] M. Long, H.J. Rack, Titanium alloys in total joint replacement a materials science perspective, Biomaterials 19 (2003) 1621–1639.
[6] J.C. Wataha, Alloys for prosthodontic restorations, J. Prosthet. Dent. 87 (2002) 351–363.
[7] M. Roach, Base metal alloys used for dental restorations and implants, Dental Clinics of North America 51 (2007) 603–627.
[8] H.H. Liu, J.H. Ni, L.H. Wu, G. He, Diffusion bonding of mismatch dental alloys, J. Biomed. Mater. Res. Part B: Appl. Biomater. 93B (2010) 39–50.
[9] H. Mancha, E. Carranza, J.I. Escalante, G. Mendoza, M. Mendez, F. Cepeda, E. Valdes, M23C6 carbide dissolution mechanisms during heat treatment of ASTM F-75 implant alloys, Metall. Mater. Trans. 32A (2001) 979–984.
[10] Z.C. Li, C.L. Li, S.B. Qiu, D.L. Wang, T.W. Guo, Biological evaluation of a new titanium alloy TAMZ as surgical implant material, Rare Metal Mater. Eng. 27 (1998) 59–62.
[11] H. Mehrer, Diffusion in Solids: Fundamentals, Methods, Materials, Diffusion-Controlled Processes, Springer-Verlag, Berlin Heidelberg, 2007, 27-205.
[12] ASM Handbook, Vol. 03: Alloy Phase Diagrams, ASM International, 1992, pp.150, 161.
[13] G. He, W. Loser, J. Eckert, In situ formed Ti–Cu–Ni–Sn–Ta nanostructure–dendrite composite with large plasticity, Acta Mater. 51 (2003) 5223–5234.
[14] G. He, J. Eckert, M. Hagiwara, Effect of Sn on microstructure and mechanical properties of Ti-base dendrite/ultrafine-structured multicomponent alloys, Metall. Mater. Trans. 35A (2004) 3605–3612.
[15] G. He, M. Hagiwara, Bimodal structured Ti-base alloy with large elasticity and low Young's modulus, Mater. Sci. Eng. C25 (2005) 290–295.